Astron. Astrophys. 319, 405–412 (1997)

ASTRONOMY
AND
ASTROPHYSICS

Radio observations of the quasar 3C395 from parsec to kiloparsec scales

L. Lara[1,2], **T.W.B. Muxlow**[3], **A. Alberdi**[2,4], **J.M. Marcaide**[5], **W. Junor**[6], **and D.J. Saikia**[7]

[1] Istituto di Radioastronomia, CNR, Via Gobetti 101, I-40129 Bologna, Italy
[2] Instituto de Astrofísica de Andalucía, CSIC, Apartado 3004, E-18080 Granada, Spain
[3] NRAL, Jodrell Bank, Macclesfield, Cheshire SK11 9DL, UK
[4] LAEFF, P.O. Box 50727, E-28080 Madrid, Spain
[5] Departamento de Astronomía y Astrofísica, Universitat de València, E-46100 Burjassot, Valencia, Spain
[6] Department of Physics and Astronomy, University of New Mexico, 800 Yale Boulevard, N.E., Albuquerque, NM 87131, USA
[7] National Centre for Radio Astrophysics, TIFR, Post Bag 3, Ganeshkhind, Pune 411007, India

Received 19 March 1996 / Accepted 1 August 1996

Abstract. We present results from global VLBI, VLBA, MERLIN and VLA observations of the quasar 3C395 at 5.0 GHz, global VLBI and VLBA observations at 8.4 GHz, and VLBI test observations at 22.2 GHz. These combinations allow us to obtain radio images with resolutions ranging from 0.2 to 200 milliarcseconds, which show the continuity of the radio structure of 3C395 from parsec to kiloparsec scales. On parsec scales we find clear signs of activity in the compact core and show that the component separations have remained unchanged since epoch 1990.8. On larger scales we confirm the existence of a very sharp bend in the jet at a distance of $\sim$ 70 mas from the core, the magnitude of which we ascribe to projection effects when the jet is viewed very close to the line of sight. We suggest that 3C395 is a double radio source viewed end-on, with two extended lobes appearing superimposed as a low brightness halo.

Key words: galaxies: jets – quasars: individual (3C395) – techniques: interferometric

1. Introduction

Current radio interferometers at centimeter wavelengths cover a range in spatial resolution from degrees to tenths of milliarcseconds (mas), allowing images to be made of radio emission over a very wide range of scale size from compact cores to the extended lobes of radio galaxies. However, in some cases with particularly complicated structures, the spatial frequency coverage from any one array may be insufficient to permit high quality imaging of emission on intermediate angular scales (tenths of arcseconds), resulting in a gap in the knowledge of the radio source structure. This limitation can be overcome by the combination of data from more than one array.

Send offprint requests to: L. Lara

3C395 (1901+319), identified with a 17th magnitude quasar at a redshift $z = 0.635$ (Gelderman & Whittle 1994), has a complex radio structure on a wide range of angular scales. Its core-jet radio structure consists, on milliarcsecond scales, of two components in a position angle (P.A.) of 118° separated $\sim$ 15 mas and stationary with respect to each other. A third weaker component is located between these two (see Lara et al. 1994, Paper I hereafter, and references therein). Low resolution images show a compact and unresolved core, and extended emission separated by $\sim$ 0.65 arcseconds in P.A.$\sim -51°$, that is, in a direction almost opposite to that of the milliarcsecond jet. Previous intermediate resolution images have suggested the presence of a bend in the radio structure between the compact and the extended emission (Saikia et al. 1990).

We observed 3C395 at 5.0 GHz, simultaneously with global Very Long Baseline Interferometry (VLBI) and the Multi Element Radio Linked Interferometer Network (MERLIN) in England, and closely in time with the Very Long Baseline Array (VLBA) in the USA and the Very Large Array (VLA) in New Mexico, USA. We have assembled combination data sets for global VLBI+MERLIN and MERLIN+VLA and have thus produced high quality images of 3C395 over a wide range of spatial resolution from 1 to 200 mas. We complement these observations with 8.4 GHz global VLBI and VLBA observations, and with a three-baseline VLBI test observation at 22.2 GHz which allows us to reach a maximum resolution of 0.2 mas, and thus to probe the details in the vicinity of the compact core. In the following discussion we assume values of H_0=100 km s^{-1} Mpc^{-1} and q_0=0.5.

Table 1. VLBI arrays

ν (GHz)	Array[1]	uv-range (Mλ)	Polarization	Epoch (yr)
5.0	Kp,Pt,La,Fd,Nl,Br	2–40	LCP	1991.6
	N,S,B,W,Cm,Kn,J,K,Y,Nl,Fd,La,Pt,Kp,O	0.8–157	LCP	1991.7
8.4	Kp,Pt,La,Fd,Nl,Br	3–60	LCP	1991.6
	N,L,S,B,K,Nl,Fd,La,Pt,Kp,Ov,Br	2–250	RCP	1992.7
22.2	L,M,K	70–450	LCP	1993.3

[1] N: 32m, Noto (Italy); L: 32m, Medicina (Italy); S: 25m, Onsala (Sweden); B: 100m, Effelsberg (Germany); W: phased array, Westerbork Synthesis Radio Telescope (The Netherlands); J: 26m, Jodrell Bank (England); Cm: 32m, Cambridge (England); Kn: 25m, Knockin (England); M: 70m, DSS63, Robledo (Spain); K: 37m, Haystack (USA); Y: 25m, VLA (USA); Nl,Fd,La,Pt,Kp,Ov,Br: 25m each, VLBA-North Liberty, -Fort Davis, -Los Alamos, -Pie Town, -Kitt Peak, -Owens Valley and -Brewster, respectively (USA); (O) 130 ft (40m), Owens Valley (USA)

2. Observations and data reduction

2.1. Global VLBI and MERLIN observations at 5.0 GHz

3C395 was observed simultaneously with global VLBI and MERLIN on September 11th 1991 at a frequency of 5.0 GHz in left circular polarization (LCP). The observing bandwidth was 2 MHz for VLBI (Mark II recording system, Clark et al. 1972) and 16 MHz for MERLIN. The strong compact sources OQ208, 1739+522 and BL Lac were observed as fringe finders for the correlation of the VLBI data, and as point source calibrators in the postprocessing.

The global VLBI array consisted of 15 antennas (see Table 1). The VLBI data were correlated in the Block II correlator at the California Institute of Technology (Caltech), and later fringe-fitted using the NRAO Astronomical Image Processing System (AIPS). The calibration of the amplitude visibilities was carried out using the Jodrell Bank OLAF package, from measured system temperatures and gain curves supplied by the individual antennas. For imaging, independent mapping procedures using the Caltech, OLAF (Pearson 1991; Muxlow et al. 1988) and AIPS packages were used and very similar results were obtained.

The MERLIN array consisted of six antennas: Jodrell-Mk2, Tabley, Darnhall, Knockin, Defford and Cambridge. Flux density calibration was performed by comparison of OQ208 and 1739+522 with the flux density calibrator 3C286 assuming a value of 7.382 Jy. For the MERLIN data, we followed standard self-calibration and mapping procedures using the OLAF and AIPS packages.

2.2. Global VLBI observations at 8.4 GHz

We observed the quasar 3C395 at 8.4 GHz in right circular polarization (RCP) on September 12th 1992 using the Mark II recording system. The 12 antennas participating in the observations are listed in Table 1. The data were correlated in the Block II correlator at Caltech. The main delay and fringe rate residuals were removed using the AIPS package and then the data were exported to the Caltech package for calibration and mapping. The data were initially calibrated using the measured system temperatures and antenna gains. The compact source 1739+522, also observed during the experiment, was then used to refine the amplitude calibration. The final image was obtained after several cycles of phase and gain self-calibration.

2.3. VLBA observations at 5.0 and 8.4 GHz

We observed 3C395 for 12 hours with six antennas of the VLBA on August 12th 1991, cycling between 5.0 and 8.4 GHz every 15 minutes (see Table 1). The data were recorded in LCP, using the Mark II recording system with a synthesized bandwidth of 2 MHz. The correlation of the data was carried out in the Block II correlator at Caltech. The data calibration was performed with the AIPS package, following a similar scheme to that described in sections 2.1 and 2.2. The sources 1739+522 and 0016+731 were used as calibrators.

2.4. VLA observations at 5.0 GHz

Observations of 3C395 were made with the VLA on August 18th 1991 over a 3 hour period. Two standard 50 MHz IFs were used with frequencies of 4835 and 4885 MHz. 3C286 was used as a flux density calibrator with assumed fluxes of 7.426 and 7.379 Jy, respectively. The phases were calibrated with the nearby source 1751+288. The calibration and mapping of the data was carried out with the AIPS package.

2.5. VLBI test observations at 22.2 GHz

Test VLBI observations of the quasar 3C395 were made on May 1st 1993 at 22.2 GHz in LCP with a three baseline array (see Table 1), using the Mark III recording system (Rogers et al. 1983) with a synthesized bandwidth of 112 MHz. The correlation and fringe fitting of the data were carried out at the Mark III correlator in Haystack (MA, USA), where the data were exported to the Caltech package format for calibration and mapping purposes. The strong point source 0954+658 was used as a flux density calibrator with an assumed flux density of 1.3 Jy. The final image was produced after several cycles of phase self-calibration.

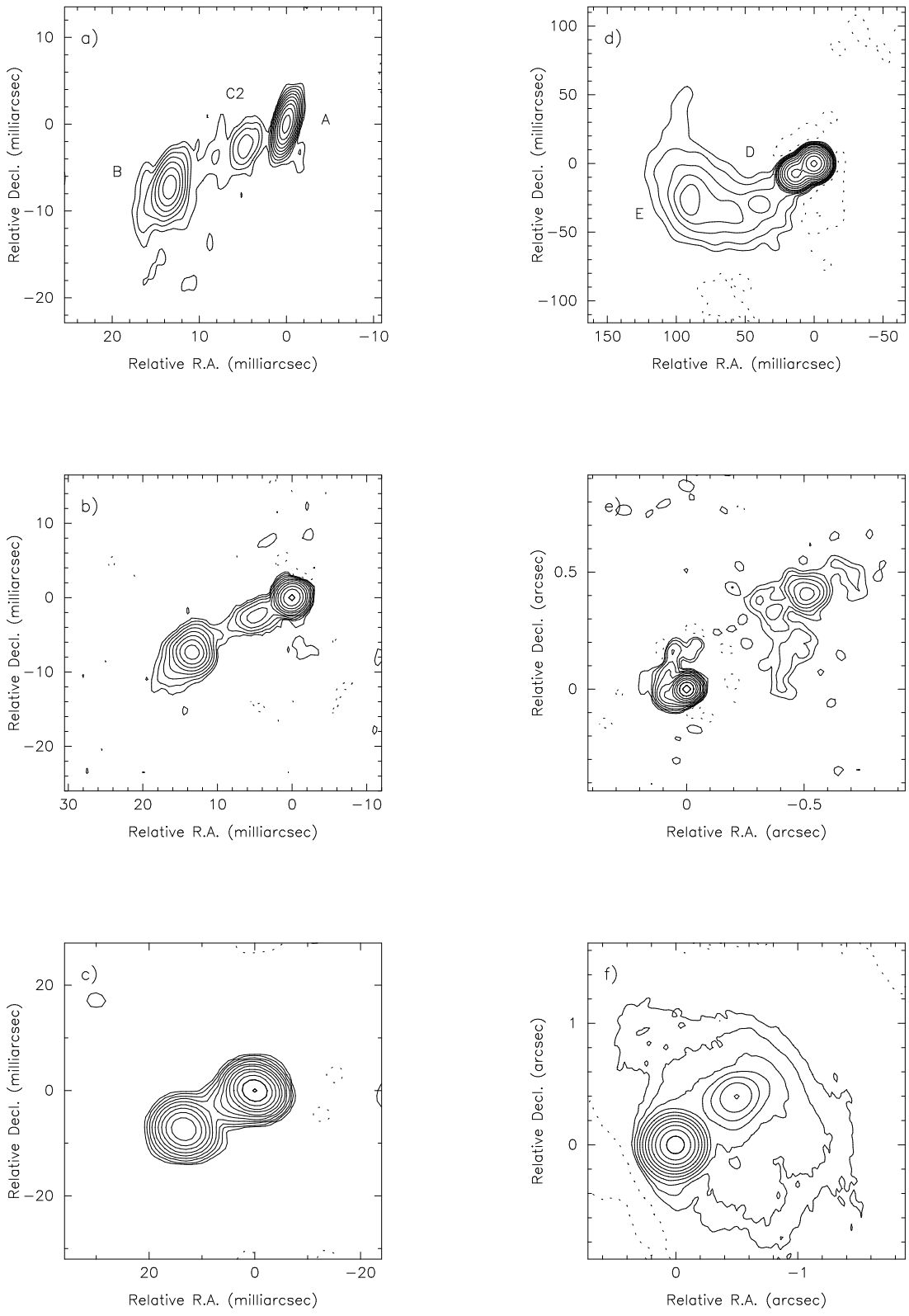

Fig. 1a–f. Maps of 3C395 at 5.0 GHz with different angular resolutions. For each map we list the type of instrument, the gaussian beam used for convolution, the map contours and the peak of brightness. **a** VLBI; 2.9 mas×1.0 mas in P.A.−12°; 0.0033 Jy/beam×(-1, 1, 2, 4, 8, 16, 32, 64, 128, 256, 360); 1.32 Jy/beam. **b** VLBI; 2 mas×2 mas; 0.0014 Jy/beam×(-1, 1, 2, 4, 8, 16, 32, 64, 128, 256, 512, 1024); 1.62 Jy/beam **c** VLBA; 4.6 mas×3.8 mas in P.A.68°; 0.009 Jy/beam×(-1, 1, 2, 4, 8, 16, 32, 64, 128, 256, 512, 1024, 2048); 1.47 Jy/beam. **d** VLBI+MERLIN; 10 mas×10 mas; 0.0007 Jy/beam×(-1, 1, 2, 4, 6, 8, 12, 16, 32, 64, 128, 256, 512, 1024, 2048); 1.66 Jy/beam. **e** MERLIN; 50 mas×50 mas; 7.4×10^{-4} Jy/beam×(-1, 1, 2, 4, 8, 16, 32, 64, 128, 256, 512, 1024); 2.02 Jy/beam. **f** MERLIN+VLA; 200 mas×200 mas; 0.0015 Jy/beam×(-1, 1, 2, 4, 8, 16, 32, 64, 128, 256, 512, 1024); 2.19 Jy/beam

Some scaling errors may be present since 0954+658 is known to be variable at this radio frequency.

3. Observational results

3.1. Maps at 5.0 GHz

In Fig. 1 we present maps of 3C395 at 5.0 GHz obtained with various array combinations, ordered in increasing angular resolution. Fig. 1a displays the global VLBI map with a restoring beam of 2.9 mas$\times$1.0 mas in P.A. -12°. (At the redshift of 3C395, 1 mas corresponds to 3.88 parsecs.) Following the same convention for component labelling as in Paper I, we find an unresolved bright feature (component A) at the western end of the structure. This is identified with the core of the radio source. Component B lies at the eastern edge of the structure $\sim$ 15.3 mas from the core in P.A. 119° (these and other values given below are derived from model-fitting). Component B appears slightly elongated towards the south-east. The feature located between components A and B is identified with component C2 reported in Paper I. It is located $\sim$ 5.4 mas from component A and is extended along P.A. 119°. Moreover, we find some evidence for emission between components C2 and B, which is supported by the global VLBI map restored with a circular gaussian beam of 2 mas (Fig. 1b). We have fitted simple elliptical gaussian models to the global-VLBI visibility data using a least-squares algorithm. Three gaussian components were needed to reproduce the visibility curves. The estimated parameters are given in Table 2, where we display the flux density (S), the angular distance from the core (D), the position angle with respect to the core (P.A.), the length of the major axis (L), the ratio between the major and the minor axes (r) and the orientation of the major axis (Φ), the latter defined in the same sense as the position angle, for each gaussian component. The errors correspond to statistical standard errors, indicating the quality of constraint after the least-squares fit. A question-mark indicates that the parameter involved is not well constrained by our data. Fig. 1c displays our 5.0 GHz VLBA map from epoch 1991.6, with an angular resolution of 4.6 mas$\times$3.8 mas in P.A. 68°. Model-fitting to these data produced results consistent with those from the global VLBI data.

We combined the self-calibrated global VLBI and MERLIN data sets. The data sets were cross-calibrated using the common baselines between the antennas at Jodrell Bank, Cambridge and Knockin. The data were self-calibrated with the high-resolution VLBI image being used as the initial source model. Several data weighting schemes were tried until we obtained a satisfactory rendition of the intermediate-scale emission. The map shown in Fig. 1d was obtained using uniform weighting, i.e. giving each uv-plane cell the same weight, with a gaussian taper of 20×10^6 λ half-width, which provided a circular restoring beam of 10 mas.

In Fig. 1d, components A and B can still be distinguished as separated features, although somewhat blended. Immediately after component B, we find a sharp decrease in the surface brightness of the jet, which however keeps its collimation and position angle with respect to the core. The intermediate scale structure is not smooth: we can identify two peaks labelled D and E in Fig. 1d. These features are identified tentatively with two components found at 0.6 GHz (see Paper I). Component D is $\sim$ 50 mas from A in P.A.$\sim$ 127° and component E appears at $\sim$ 96 mas from A in P.A.$\sim$ 107°. Near component D, at about $\sim$ 70 mas from the core, the jet starts bending towards the north. The surface brightness of the radio jet falls rapidly beyond component E.

In Fig. 1e we present the MERLIN map, with a resolution of 50 mas. The VLBI structure is unresolved, appearing as a single strong component with a peak brightness of 2.0 Jy/beam. From this component, a jet emerges in P.A. $\sim$ 111°, consistent with the position angle of the milliarcsecond scale jet, but the jet soon after bends strongly by $\sim$ 170° towards the northeast, with a local peak $\sim$ 0.65 arcseconds and P.A.$\sim -51°$ with respect to the central component.

Fig. 1f displays the map resulting from the combination of the MERLIN and VLA arrays, with a resolution of 200 mas. It shows two main components, corresponding to the core emission, which is unresolved, and to the peak of the extended emission, all embedded in a diffuse envelope.

3.2. VLBI map at 8.4 GHz

In Fig. 2 we show the map of 3C395 made at 8.4 GHz from global VLBI observations in epoch 1992.7. We identify components A and B, and a weak component C2 between the two. We do not detect any extended emission. As with the results at 5.0 GHz, we initially model-fitted to our VLBI data with a three gaussian component model, but the longer baselines could not be fitted satisfactorily. Better results were obtained by splitting component A in two sub-components, A1 and A2, separated by 0.7 mas in P.A. 128°. This sub-structure becomes visible if the image is super-resolved by restoring with a smaller circular beam. The results of the fit are displayed in Table 2. From this analysis, we derive a separation between component C2 and A1 of 5.7 mas. In order to compare this estimate with the results at 5.0 GHz, we have computed the distance from C2 to the centre of brightness of A1 and A2. For the latter we find a value of 5.3 mas, which is fully consistent with the result at 5.0 GHz. We find similarly consistent results for the separation of components A and B at 5.0 and 8.4 GHz respectively.

Our 8.4 GHz VLBA map, convolved with a gaussian beam of size 2.9 mas$\times$2.6 mas in P.A. 65°, does not provide further structural information at this frequency. Due to the lower resolution provided by the reduced VLBA array, a similar model-fitting analysis needs only of three gaussian components to provide a satisfactory fit to the visibility data. The results for components A and B are displayed in Table 2. Results for component C2 were not well constrained by the data.

3.3. Spectral-index map between 8.4 and 5.0 GHz

We have taken advantage of simultaneous VLBA observations at 8.4 and 5.0 GHz in 1991.6 and have constructed a spectral-

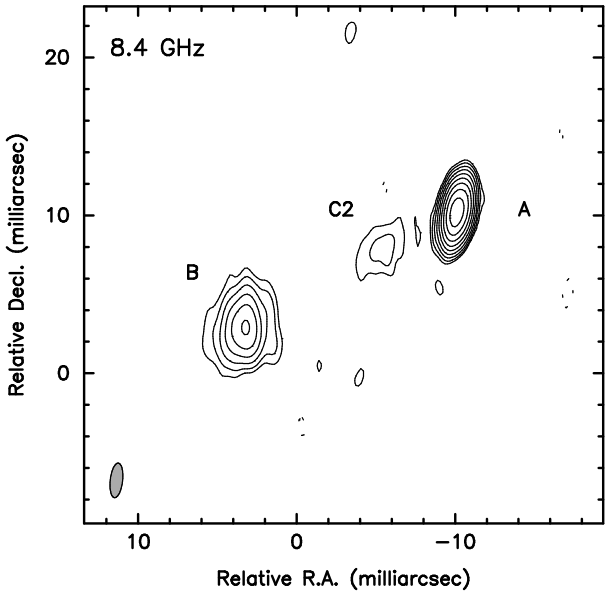

Fig. 2. VLBI map of 3C395 at 8.4 GHz from epoch 1992.7. An elliptical gaussian beam of 2.2 mas×0.8 mas with major axis along P.A. $-6°$ has been used to obtain the image. The contours represent -0.25, 0.25, 0.5, 1, 2, 4, 8, 16, 32, and 64% of the peak brightness of 1.2 Jy/beam. The flux density in the VLBI map is 1.88 Jy

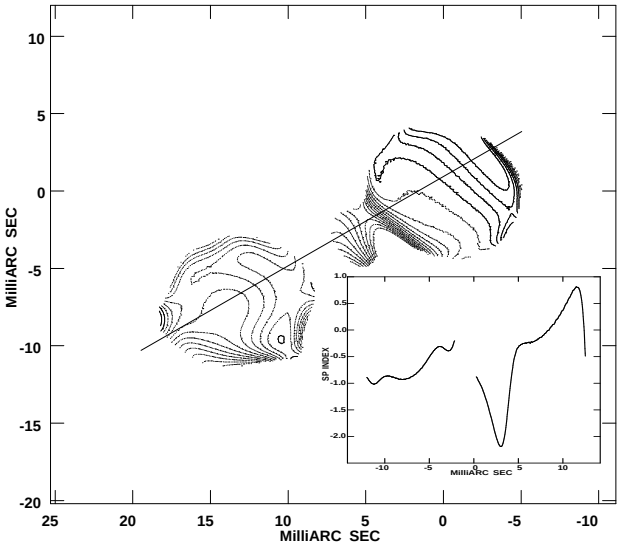

Fig. 3. Spectral-index map of 3C395 between 8.4 and 5.0 GHz obtained from VLBA observations at epoch 1991.6. The one-dimensional curve in the inset represents the numerical values of the spectral index (α) along the solid line drawn on the map from northwest to southeast. Contours of the spectral index range from -2.4 to 0.6 with intervals of 0.2. (α is defined so that the flux density $S \propto \nu^{\alpha}$)

index map of 3C395. The images were registered by the peak of brightness of component B in the two maps. Component B is optically thin between these two frequencies (Paper I), and is thus not subject to opacity effects. In order to align component B in both maps, we have shifted the peak of brightness of the 5 GHz map by 0.14 mas in a position angle of 135° with respect to the peak of brightness of the 8.4 GHz map. Both images were smoothed to the same resolution of 3.5 mas×2.9 mas in P.A. 68° (75% the size of the synthesized 5.0 GHz beam). The resulting spectral-index map is displayed in Fig. 3, together with a one dimensional slice along the jet main position angle. The map clearly shows an optically thick core with a spectral index gradient which is aligned with the position angle of the substructure in component A. In addition, the fact the spectral index of component B appears flatter towards the west can be explained by curvature of the jet towards the observer's line of sight, which would result in a greater column depth through the radiating material in the western side of this component.

3.4. Results at 22.2 GHz

The map from our data set at 22.2 GHz is displayed in Fig. 4. We find a core-jet structure consisting of an unresolved component at the western extreme of the brightness distribution, and two additional components directed along P.A.$\sim$ 140°, a value which differs significantly from the accepted position angle of the parsec-scale jet (118°). In spite of the reduced uv-coverage, we are confident that the two stronger components are real. These correspond to the double structure found in component A at 8.4 GHz. We note that all the structure displayed in Fig. 4 fits inside component A in Fig. 1a or Fig 2. The data at 22.2 GHz are not sensitive enough to detect components B or C2.

4. Discussion

4.1. The compact core of 3C395

The variability in the flux density of component A is evidence for activity in the compact core of 3C395. We measure a flux density of 1.5 Jy for this component at 5.0 GHz in 1991.7 (1.2 Jy in 1986.9; Simon et al. 1988b) and, at 8.4 GHz, 1.5 Jy in 1991.6 and 1.6 Jy in 1992.7 (1.3 Jy in 1990.8; Paper I). We note that component A is not a well-defined homogeneous component, but shows a complex core-jet structure with at least two main features, A1 and A2. The position of A1 at the edge of the brightness distribution, its compactness, and flat spectral index ($\alpha_{8.4}^{22.2} = -0.2$), suggest that this is the true core of the radio source.

The nature of sub-component A2 is unknown. It could be either a bend in the inner part of the jet towards the direction of the observer (see Paper I), or a newly emerging component. In the former case, the emission from a compressive shock in the jet flow located at the position of the bend would be enhanced by Doppler boosting. This would give rise to an increase in the flux density in this region. After passing through the bend region the flux density would decrease as the material moves downstream. In VLBI observations with angular resolutions poorer than 1 mas, we would not resolve this region, but would observe such changes as the variability of a single core component A. Thus, possible bends in the vicinity of the core of 3C395 would act as emission amplifiers, which would allow us to detect flux

Table 2. Gaussian fit parameters of the compact structure

Component	S (Jy)	D (mas)	P.A. (deg)	L (mas)	r	Φ (deg)	ν (GHz)	Epoch (yr)
A	1.55±0.01	–	–	0.90±0.02	0.2±?	123±2	8.4	1991.6
A	1.49±0.01	–	–	0.77±0.02	0.36±0.02	135±2	5.0	1991.7
A1	0.57±0.01	0	0	0.34±0.01	0.48±0.06	126±3	8.4	1992.7
A2	1.04±0.01	0.67±0.01	127.7±0.2	0.36±0.01	0.53±0.03	125±1	8.4	1992.7
B	0.29±0.01	15.36±0.04	119±?	1.8±0.1	0.9±0.1	135±?	8.4	1991.6
B	0.41±0.01	15.25±0.03	118.6±0.1	2.2±0.1	0.66±0.05	-1±5	5.0	1991.7
B	0.25±0.01	15.75±0.03	119.0±0.1	1.6±0.1	0.90±0.06	12±?	8.4	1992.7
C2	0.06±0.01	5.4±0.2	119±2	2.9±0.7	0.4±?	130±40	5.0	1991.7
C2	0.02±0.01	5.7±0.5	117±3	2.8±?	0.3±?	125±25	8.4	1992.7

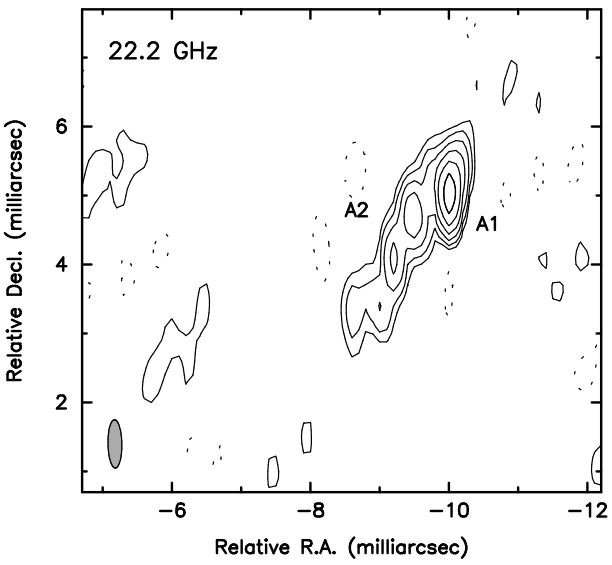

Fig. 4. VLBI map of 3C395 at 22.2 GHz from epoch 1993.3. An elliptical gaussian beam of 0.7 mas×0.2 mas with major axis along P.A. 1° has been used to obtain the image. The contours represent -2, 2, 4, 8, 16, 32, and 64% of the peak brightness of 0.31 Jy/beam. The flux density in the VLBI map is 0.63 Jy

density variations caused by weak shock waves. Once ejected from the core region, the corresponding components would be below current detection limits. This mechanism could explain how the flux density variability in the core of 3C395, ultimately associated with the ejection of new components (Valtaoja et al. 1988), does not result in structural variations.

4.2. Component C2

Taking account of the differing angular resolution of our images at 5.0 and 8.4 GHz, we find that the separation between component A and C2 has remained constant between 1991.7 and 1992.7. Additionally, a detailed comparison of the map in Fig. 2 with a map from epoch 1990.8 at 8.4 GHz (Paper I), and the results derived from model-fitting, allow us to extend the stationary character of component C2 back to 1990.8.

We have no evidence to suggest that the stationary component C2 can be identified with component C1 found in previous VLBI observations. In fact, C1 and C2 could be two different components affected by similar kinematical processes (Paper I). Between 1979.9, 1983.3 and 1985.4, component C1 was observed to move superluminally from the core with an apparent velocity of 0.64 mas/yr (Simon et al. 1988a). However, between 1985.4 and 1986.9, it showed a strong apparent deceleration (Simon et al. 1988b). Invoking a change in the orientation of a conically expanding uniform jet containing a moving shock cannot explain such a dramatic deceleration. The large changes in the geometry required to produce such a deceleration would also demand strong variations in the Doppler boosting factor, and consequently, in the flux density of the component. Such flux density variations have not been observed.

Hardee (1990) suggests additional superluminal mechanisms related to the existence of shocked helical structures associated with Kelvin-Helmholtz (K-H) instabilities in jets. A planar shock wave with a constant subluminal velocity propagating down an unstable jet could produce an observable radio knot resulting from its interaction with a K-H helical structure. This feature would be located at the intersection point between the helical structure and the planar shock, and would propagate with a phase velocity which could be superluminal. The deceleration of such a feature would not be associated with a variation in brightness since the change of velocity would be the result of a phase effect and not of a change in the orientation of the stream lines of the fluid with respect to the line of sight. This could be the case for component C1, and perhaps C2 (see also Rosen 1990).

4.3. Component B

First detected in 1978, component B has remained stationary with respect to the core of 3C395, with minor changes in its relative position probably due to displacements of the peak of brightness of component A. Considering the available data on the position of component B at different epochs and frequencies, we find (by means of a least-squares fit) a limit to its motion relative to the core of -0.01 ± 0.01 mas/yr, which corresponds to an apparent velocity of (-0.2 ± 0.2)c. The flux density mea-

sured for this component at 5.0 GHz (S_{5GHz} = 0.41 Jy), its spectral index ($\alpha_{5.0}^{8.4} = -0.74$) and its size, are fully consistent with previous observations. The stationary character of component B can be explained by Doppler boosting of the radiation from a portion of a relativistic jet which is directed towards the observer (see Paper I). In addition, the rapid decrease in the surface brightness of the jet immediately after the position of component B (Fig. 1d) can be explained by a subsequent re-orientation of the jet towards less favored directions.

4.4. Large scale structure of 3C395

The geometry of the jet of 3C395 beyond the structure observed with VLBI was unclear until Saikia et al. (1990), from MERLIN observations, suggested the existence of a sharp bend in the jet giving rise to a dramatic change in position angle from the milliarcsecond to the arcsecond-scale structure. Our observations confirm the existence of this bend, which appears to start at a distance of ∼70 mas from the VLBI core. This kind of sharp bend seen in projection on the plane of the sky is a strong indication of a favorable orientation of the jet towards the observer. In fact, when the angle between the jet and the observer's line of sight is smaller than the intrinsic bending angle of the jet, curvatures of up to 180° can be observed (Muxlow & Garrington 1991). This argument is also consistent with the orientation angle derived from the apparent superluminal velocity of component C1 measured in previous VLBI observations (Simon et al. 1988a), or with the results from numerical simulations in Paper I.

We find no evidence of a counter-jet in any of our maps, even at a dynamic range of 2700:1 (Fig. 1e). (The dynamic range is defined as the ratio between the peak brightness and the lowest contour value which was set at 4 times the root mean square of the residuals in the image). Although the one-sidedness of the jet could be an intrinsic property of 3C395, the orientation with respect to the observer (for which we have argued above) suggests that there are two oppositely-directed relativistic jets, one of which is Doppler-boosted to the observer's advantage. The lack of detection of a counter-jet indicate that the relativistic velocities persist out to kiloparsec scales.

We do not find the two spatially separated extended lobes of emission, typical of large-scale radio structures in radio galaxies and most quasars. We suggest that 3C395 is an end-on radio galaxy, so that the lobes at the end of the jet and counter-jet appear superimposed, resulting in the halo of low-brightness emission seen in Fig. 1f. Comparable resolution observations at lower radio frequencies could test this hypothesis.

5. Conclusions

The combination of data from different radio interferometers has allowed us to obtain new images of the radio structure of the quasar 3C395 with spatial resolutions ranging from 0.2 to 200 mas. With this wide range of resolutions, we demonstrate the continuity of the jet of this radio source from parsec to kiloparsec scales. Our main results, ordered in increasing linear scales, are as follows:

Few parsecs: The component traditionally identified with the compact core of 3C395 (component A) presents clear signs of activity, and appears resolved with VLBI observations at high frequencies. At 8.4 GHz this component is marginally resolved into a double structure while at 22.2 GHz a complex core-jet structure is found. The orientation of the resolved structure in component A appears to depart significantly from the overall position angle of the milliarcsecond-scale jet, 118°. It is not clear if the sub-structure A2 in component A is due to a new emerging component, or to bends close to the active core. Detailed VLBI observations at 22.2 GHz, and space VLBI observations should provide the necessary resolution to study the details in the vicinity of the very compact core of 3C395.

Tens of parsecs: At this scale, we find radio structure consisting of three components whose relative positions have, within measurements errors, remained unchanged since 1990.8. This result is in sharp contrast with the fast superluminal motion once reported for 3C395. A model involving the interaction of planar shock waves with K-H helical structures in a conical jet appears able to explain both the deceleration of the apparent superluminal component C1, together with its unchanging flux density, and the current stationary position of component C2.

Hundreds of parsecs: We confirm the existence of a sharp bend in the jet of 3C395 connecting the parsec-scale and the kiloparsec-scale structures. This bend takes place at ∼ 70 mas from the core.

Kiloparsecs: The sharp jet curvature and the small angular size of 3C395, together with its previous superluminal motion, argue in favour of a very close overall orientation of the jet of this radio source with respect to the observer's line of sight. In accordance with unified schemes, we suggest that 3C395 is a radio galaxy seen end-on, such that the two extended lobes appear superimposed. This hypothesis is supported by the diffuse halo of emission detected in our lowest resolution image at 5.0 GHz. The absence of a counter-jet (within sensitivity limits) even at kiloparsec scales indicates that the plasma flow remains relativistic along the entire length of the jet until it begins finally to slow as it enters the region of the knot ∼0.65 arcsecond to the northwest of the core which we suggest is associated with a hot-spot in the nearside outer lobe structure.

Acknowledgements. We wish to thank the EVN and US VLBI networks, and the staff of the different observatories for their contributions to the observations. We want to thank the CIT Block II and Haystack staff at the correlators, and P. Elósegui, for their efforts during the correlation of the data. The VLA and the VLBA are facilities of the National Radio Astronomy Observatory operated under agreement with Associated Universities Inc. MERLIN is a UK national facility operated by the University of Manchester on behalf of PPARC. L.L. thanks Prof. R.D. Davies for making a visit to Jodrell Bank possible, and acknowledges support from a postdoctoral CSIC grant. This work has been

partially supported by the Spanish DGICYT grant PB89-0009 and by an Acción Especial from the CSIC.

References

Clark B.G., Weimer R., Weinreb S., 1972, NRAO report 118
Gelderman R., Whittle M., 1994, ApJS 91, 491
Hardee P.E., 1990. In: Zensus J.A., Pearson T.J. (eds.), Parsec-scale radio jets, Cambridge University Press, p.266
Lara L., Alberdi A., Marcaide J.M., Muxlow T.W.B., 1994, A&A 285, 393
Muxlow T.W.B., Garrington S.T., 1991, In: Beams and Jets in Astrophysics, Hughes P.A. (eds.), Cambridge University Press, p.52
Muxlow T.W.B., Junor W., Spencer R.E., et al., 1988, In: Reid M.J., Moran J.M. (eds.) Proc. IAU Symp. 129, The Impact of VLBI on Astrophysics and Geophysics, Kluwer Academic Publishers, p.131
Pearson T.J., 1991, BAAS 23, 991
Rogers A.E.E., Capallo R.J., Hinteregger H.F., et al., 1983, Science 219, 51
Rosen A., 1990, ApJ 359, 296
Saikia D.J., Muxlow T.W.B., Junor W., 1990, MNRAS 245, 503
Simon R.S., Hall J., Johnston K.J., et al., 1988a, ApJ 326, L5
Simon R.S., Johnston K.J., Spencer J.H., 1988b, In: Reid M.J., Moran J.M. (eds.) Proc. IAU Symp. 129, The Impact of VLBI on Astrophysics and Geophysics, Kluwer Academic Publishers, p.21
Valtaoja E., Haarala S., Lehto H., et al., 1988, A&A 203, 1

This article was processed by the author using Springer-Verlag LaTeX A&A style file *L-AA* version 3.